J Mol Model (2013) 19:1429–1434
DOI 10.1007/s00894-012-1701-z

ORIGINAL PAPER

Molecular vibrational spectroscopy characterization of epoxy graphene oxide from density functional calculations

Bo Liu · Hongjuan Sun · Tongjiang Peng · Guangfu Ji

Received: 13 September 2012 / Accepted: 19 November 2012 / Published online: 9 December 2012

Abstract To further understand the structure of graphene oxide, several structures of graphene oxide were systematically investigated using density functional theory (DFT). Our models consisted of a hexagonal in-plane structure of graphene with epoxy groups, and different oxidation levels. We found that different arrangements of these units yielded a range of vibrational spectra. Raman positions of the D and G bands depend sensitively on the local atomic configurations. Both structure energy and spectra computations indicate that the oxidation functional groups are energetically favorable to aggregate together and to be close to one another on the opposite side of graphene surface.

Keywords Epoxy groups · First-principle calculations · Graphene oxide · Molecular vibrational modes · Raman spectrum

Introduction

Graphene, a two-dimensional crystal, is comprised of carbon atoms tightly packed into a hexagonal honeycomb lattice. For the perfect crystal structure, it has unique physical properties, such as mechanical, electrical, optical and thermal properties [1–7]. Graphene is a basic building unit for graphitic materials. It can be wrapped into zero-dimensional fullerene, rolled into one-dimensional carbon nanotubes and stacked into three-dimensional graphite [8]. Since 2004, Novoselov et al. [3] have succeeded in producing the monolayer graphene by micro-mechanical striping method, which broke the traditional cognitive that strictly two-dimensional crystals were thermodynamically unstable and could not exist [9, 10]. The successful production of graphene has opened a new era and generated renewed interest in carbon compounds.

Due to the unique electronic structure of graphene, the σ bond with sp^2 hybrid mode of in-plane makes it of a higher structural stability. And the delocalization of π bond of out-plane is important for appropriate functional group modification, which will make of it a system with important chemical activity. Graphene oxide (GO) is one of the important derivatives of graphene. Like graphene, it possesses excellent physicochemical properties for the decorated oxygen-containing functional groups. Types of functional groups, contents and relative density in the structure play an important regulatory role. Lahaye [11] and Dinh [12] have studied changes in the relative position of functional groups and their impacts on the structure stability of GO. Fuente [13] calculated the infrared spectral characteristics of the GO. Kudin [14] used DFT methods to calculate the Raman spectra of GO, and compared with the experimental Raman spectra to study the structural changes. Because of the complexity and diversity of oxygen groups, it has not worked out a unified structure of graphene oxide.

Infrared absorption and Raman scattering spectrum is the fingerprint of the matter structure. They are directly related to the symmetry of the molecular structure. The infrared spectrum reflects types of functional groups, quantity and their associated molecular vibrational modes, and the

B. Liu
Department of Science,
Southwest University of Science and Technology,
Mianyang 621010 Sichuan Province, People's Republic of China

H. Sun (✉) · T. Peng
Institute of Mineral Materials and Application,
Southwest University of Science and Technology,
Mianyang 621010 Sichuan Province, People's Republic of China
e-mail: sunhongjuan@swust.edu.cn

G. Ji
China Academy of Engineering Physics, Mianyang 621010
Sichuan Province, People's Republic of China

Raman spectrum is used to identify contents of different chemical bonds and disorder in the structure of GO. Oxidation of graphite is generally considered to be achieved through the intermediate formation of epoxy [15]. Pandey observed GO has local crystal structure with oxygen atoms regularly arranged on the carbon atom plane in the form of epoxy groups through ultra-high vacuum scanning tunneling microscope [16]. Li found that line defects in GO are arranged into columns of epoxy matrix structure [17]. Based on previous research on properties of GO and the structure model proposed by Hoffman [18], we use super unit cell to build periodic variants, and apply DFT to study the effect of numbers and arrangements of epoxy in the GO structure on the molecular vibrational spectroscopy.

Models and calculation methods

Experimental data have shown that the C/O ratio of saturated GO is close to 2:1 [19, 20]. Therefore, based on the ratio, we construct the GO models with different numbers of epoxy groups and different arrangements. To avoid the effect of the finite edges, we adopt a periodic supercell approach, using a 2×2×1 hexagonal supercell containing eight carbon atoms. With principles of permutations and combinations, 19 kinds of graphene oxide models were applied. They are displayed in Fig. 1.

The first-principles total energy pseudopotential calculations are based on the density functional theory with the local-density-approximation (LDA) functional as implemented in the CASTEP package [21, 22]. The form of Ceperley and Alder as parametrized by Perdew and Zunger is used for the exchange-correlation functional [23, 24]. Since LDA is known to be more accurate to describe interlayer coupling in graphitic materials and other van der waals systems [20, 25, 26]. Moreover, structural properties of GO have been achieved successfully by using LDA [27–30]. The interactions between core region and valence electrons are described by the norm-conserving pseudo potentials [31], and the cut-off energy for the plane-wave basis expansion is 830 eV. Periodic supercells are used, in the Z

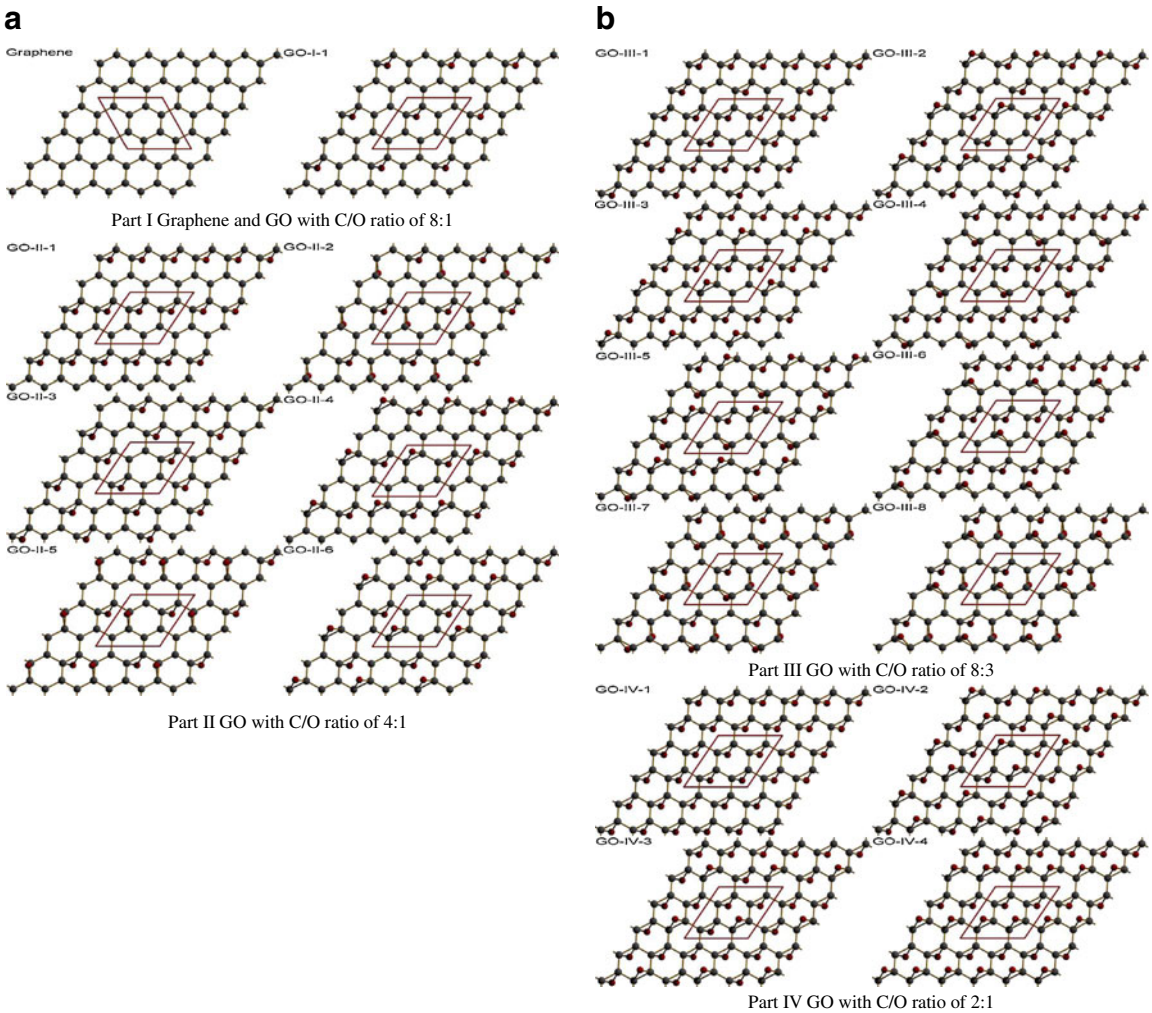

Fig. 1 GO models with different C/O ratio

direction a 15 Å-thick vacuum region to separate the GO sheet from adjacent images. The first Brillouin zone samplings are performed using sufficient k-points generated by the Monkhorst-pack scheme that ensures total energy convergence to 5×10^{-6}eV [32]. Structural parameters are relaxed using the Broyden Fletcher Goldfarb Shanno (BFGS) minimization method [33]. The structure is relaxed until the force on each atom is less than 0.01 eV $Å^{-1}$ and the stress on the cell less than 0.02 GPa.

Results and discussion

After the relaxation process, the carbon atom plane of optimized structure was warped with different degrees, keeping the topology of the six-member network ring, and our calculation is in agreement with the results of Lahaye and Dinh [11, 12]. The foldings were caused by the stress induced from the epoxy on both sides of the carbon plane, and these statuses helped to reduce the whole system energy to maintain the structure stability. The bond length of C-C in optimization structures is close to that of diamond, which further confirmed the sp^2 hybrid bonds were gradually changed to the sp^3 hybrid bonds and the newly increased epoxy groups weakened the conjugated π bond intensity.

Structural stability of GO

To find out the stable GO structures and how the functional groups prefer to arrange, we have calculated the energy change associated with grouping the epoxy. For different oxidized GO, we use the models with variable C/O ratio to calculate.

The energy for the fully relaxed atomic arrangements is indicated. As shown in Fig. 2, the energy of model GO-II-4, GO-III-5 and GO-IV-2 is the lowest for the C/O ratio of 4:1, 8:3 and 2:1, respectively. For models with C/O ratio of 4:1, it is found that the configuration of GO-II-4 is 0.66 eV lower in energy than that of the second favorable structure (GO-II-6). With the increase of oxidation, it also indicates that models with epoxy groups on the opposite direction of graphene surface are more stable in energy than that of models with epoxy groups on the same side. Besides, the energy is lowered considerably when epoxy groups are aggregated together. Particularly, the most energetically favorable configurations are those models with the functional groups staying next to one another, but at the opposite side of the carbon sheet. This confirms the important experimental results inferred from the NMR data that the functional groups must be very close to one another [34–36]. However, the arrangements that the functional groups are attached to carbon plane in the same direction and the functional groups are located far away from each other will lead to more tension in the carbon grid and it increases the total energy. Clearly, the structure of GO is preferable in energy, and the results in Fig. 2 indicate that these adsorbed groups prefer to stay close to each other on the opposite side of graphene surface. One of the reasons why these functional groups prefer to aggregate together may be the cancellation of vertical structural distortion when these functional groups are located on both sides of the graphene sheet.

Analysis of molecular vibrational modes

Combining the group-theoretical analysis and molecular structure symmetry, we performed the reducible representation character and vibrational modes. Results are listed in Table 1.

It is clear that the symmetry of graphene is D_{6h} group. Apart from three translational normal modes, graphene has three optical normal modes at the Brillouin zone center. The A_{2u} and E_{1u} representations are translations of the plane; the B_{2g} mode is an optical phonon where the carbon atoms move perpendicular to the graphene plane. And the E_{2g} is a doubly degenerate in-plane optical vibration. Among these modes, only the E_{2g} mode is Raman-active. With respect to graphene, the epoxy groups on the graphene surface decrease the symmetry of structure. Because the point group of each GO model displayed in Fig. 1 is the sub-group of D_{6h}. From Table 1, it can be concluded that the active distributions of vibrational modes are greatly affected by

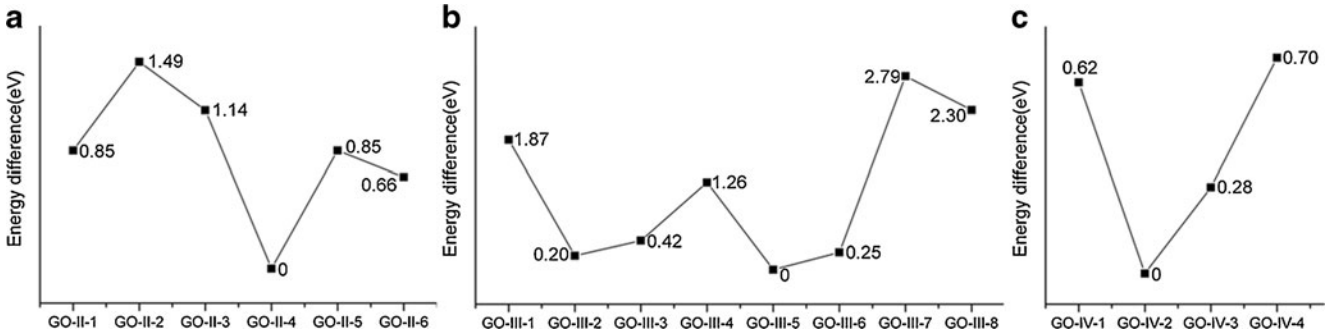

Fig. 2 Energy differences of graphene oxide with different oxidation

Table 1 Vibrational modes, distributions and active of graphene oxide

No.	Symmetry	Vibrational modes and distributions	IR active	Raman active
Graphene	D_{6h}	$B_{2g}+E_{2g}+A_{2u}+E_{1u}$	A_{2u},E_{1u}	E_{2g}
GO-I-1	C_{2v}	$6B_2+8A_1+B_1+5A_2$	A_1, A_2, B_1, B_2	A_1, A_2, B_1, B_2
GO-II-1	C_2	15A+15B	A, B	A, B
GO-II-2	C_s	15A′+15A″	A′, A″	A′, A″
GO-II-3	C_{2v}	$3B_1+5A_1+5B_2+2A_2$	A_1, A_2, B_1, B_2	A_1, A_2, B_1, B_2
GO-II-4	C_{2h}	$8B_u+7A_u+8B_g+7A_g$	A_g, A_u, B_g, B_u	A_g, B_g
GO-II-5	C_2	15B+15A	A, B	A, B
GO-II-6	D_{2h}	$5B_{1u}+4B_{3u}+4B_{2u}+5B_{3g}+3B_{2g}+4A_g+3B_{1g}+2A_u$	B_{1g}, B_{2g}, B_{3g}, B_{1u}, B_{2u}, B_{3u}	A_g, B_{1g}, B_{2g}, B_{3g}
GO-III-1	C_{2v}	$8B_2+10B_1+9A_1+6A_2$	A_1, A_2, B_1, B_2	A_1, A_2, B_1, B_2
GO-III-2	C_{2v}	$8B_2+10B_1+9A_1+6A_2$	A_1, A_2, B_1, B_2	A_1, A_2, B_1, B_2
GO-III-3	C_2	18B+15A	A, B	A, B
GO-III-4	C_2	16A+17B	A, B	A, B
GO-III-5	C_1	A	A	A
GO-III-6	C_2	16A+17B	A, B	A, B
GO-III-7	C_{3v}	$11E+6A_1+5A_2$	A_1, A_2, E	A_1, E
GO-III-8	C_s	16A″+17A′	A′, A″	A′, A″
GO-IV-1	C_{2v}	$3B_1+2B_2+3A_1+A_2$	A_1, A_2, B_1, B_2	A_1, A_2, B_1, B_2
GO-IV-2	D_{2h}	$2B_{2u}+3B_{1u}+3B_{3u}+2B_{3g}+A_u+3B_{2g}+3A_g+B_{1g}$	B_{1g}, B_{2g}, B_{3g}, B_{1u}, B_{2u}, B_{3u}	A_g, B_{1g}, B_{2g}, B_{3g}
GO-IV-3	C_{2v}	$11B_1+9B_2+10A_1+6A_2$	A_1, A_2, B_1, B_2	A_1, A_2, B_1, B_2
GO-IV-4	C_{2h}	$5B_u+4A_u+5B_g+4A_g$	A_g, A_u, B_g, B_u	A_g, B_g

the arrangement of epoxy groups. Along with the oxidation process, the vibrational modes of Raman active increase. The lower symmetry of structure as compared to graphene (D_{6h}) leads to a splitting of most modes, which is indeed observed by the large number of peaks in Fig. 4 as compared to the Raman spectrum of graphene.

Compared with the monolayer graphene results, distinct feature can be identified for GO. There are more Raman active modes in GO. These modes arise from the effect of epoxy groups. Our GO models have various point group symmetries for the Γ point. The monolayer graphene possesses the D_{6h} symmetry. It reduces to C_{2h} for the model GO-II-4, C_1 for the model GO-III-5, C_2 for the model GO-III-6 and D_{2h} for the model GO-IV-2. Correspondingly, their high optical zone-center modes are of different mode symmetries: E_{2g} mode in graphene evolves into A_g+B_g for the model GO-II-4, A+B for the model GO-III-6, and A_g+B_{1g} for the model GO-IV-2. The A_g, B_g, A, B and B_{1g} modes are both Raman and IR active. Therefore, a complete picture of the zone-center modes can be obtained from a combination of Raman and IR measurements, and the mode splitting provides significant information about the structure geometry.

Analysis of Raman spectra

The Raman spectrum is very sensitive to change of the atomic structure in carbon materials. Therefore, it is the most effective tool to study surface microstructure and the vibrational properties of graphene oxide, and the Raman spectrum can also characterize the ordered and disordered crystal structures by distinguishing Raman shifts and shapes of Raman peaks. Progress has been made in the structural characterization of the GO on the theoretical side [11, 20, 37]. However, there is general lacking of a way from calculation Raman spectroscopy to reflect the local structures of GO.

Experimental studies supply vital perspectives into the structural characterization of GO [14, 38, 39]. There are two prominent bands in Raman spectrum of GO. One characteristic band around 1585 cm^{-1} is called G band, and the other band around 1350 cm^{-1} is called D band. In the review of previous studies [40–42], the G band is assigned to the doubly degenerate zone center E_{2g} mode, referring to the vibration of sp^2-bonded carbon atoms in a two-dimensional hexagonal lattice, and the D band is related to the K-point phonons of A_{1g} symmetry which is assigned to local defects and structural imperfections induced by functional groups on the graphene sheets. Therefore, the D band is not observed in the defect-free graphene but discovered in the defected graphene and GO. For all the local GO structures shown in Fig. 1, we have done the first order calculated Raman spectrum of graphene in Fig. 3 and the Raman spectra of GO in Fig. 4. The Raman spectra are focused on the intermediate wave number region (1000–2000 cm^{-1}) that is associated with the vibration of carbon atoms.

For comparison, we first calculated the Raman spectrum of graphene (Fig. 3). From our LDA calculations, The Raman spectrum of graphene, as expected, displays a prominent G

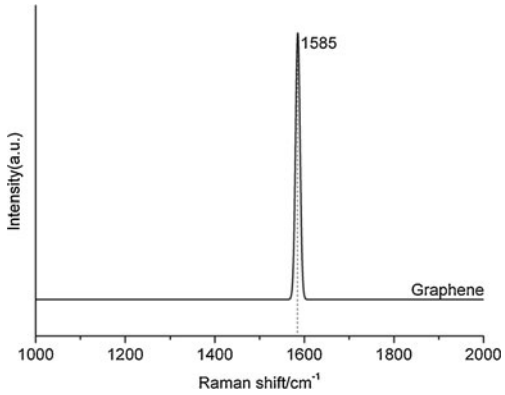

Fig. 3 Raman spectrum of graphene

peak as the only feature at 1585 cm^{-1}, corresponding to the first-order scattering of the E_{2g} mode. Our calculation data agree remarkably well with the experimentally observed G band at 1585 cm^{-1} [43, 44]. With the addition of epoxy groups on the graphene surface, a series of new Raman active bands appears (Fig. 4), demonstrating the substantial contribution of the epoxy groups to the Raman spectra. This may be attributed to the lower symmetry which leads to the splitting of most modes. The vibrational frequencies in the range 1300–1400 cm^{-1} can be correlated with D band. With an 80 cm^{-1} Gaussian broadening, some of them are in excellent agreement with the experimental values. As the Raman spectrum of graphene shown in Fig. 3, the D band is Raman inactive. When the epoxy groups are arranged on the graphene surface, the structural symmetry is broken. Thus, the D band is activated by the presence of functional groups in GO and causes a change in the selection rules. In Fig. 4 the band associated around 1585 cm^{-1} is designated as G band. Some G bands of the spectra show shift of varying degrees in the G band to higher energy regions, with respect to graphene. In particular, it is more significant in higher oxygen coverage. There are two possible explanations for the blue shift of G band. One is overlap of the G band with the D band (locating at 1620 cm^{-1}) that becomes active due to structural imperfections from the attachment of functional groups on the carbon sheet. And the other is the presence of isolated conjugate π bonds separated by functional groups on the carbon network of GO [14, 40]. The spectra of model GO-II-4, GO-III-5 and GO-III-6, and GO-IV-2 are more close to the experimental data for the C/O ratio of 4:1, 8:3 and 2:1, respectively. The Raman spectrum of GO-II-4 contains both G and D bands (at 1585 and 1370 cm^{-1}, respectively), and the D/G intensity ratio is the highest in other GO models. These results can be compared with the experimental values for reduced GO [38]. In the Raman spectrum of GO-III-5, the G band is broadened and shifted to 1602 cm^{-1}, and the D band is at 1330 cm^{-1}. This observation is consistent with experiment [39]. From the above analysis of vibrational modes, we know that these G bands are caused by those modes split from the E_{2g}

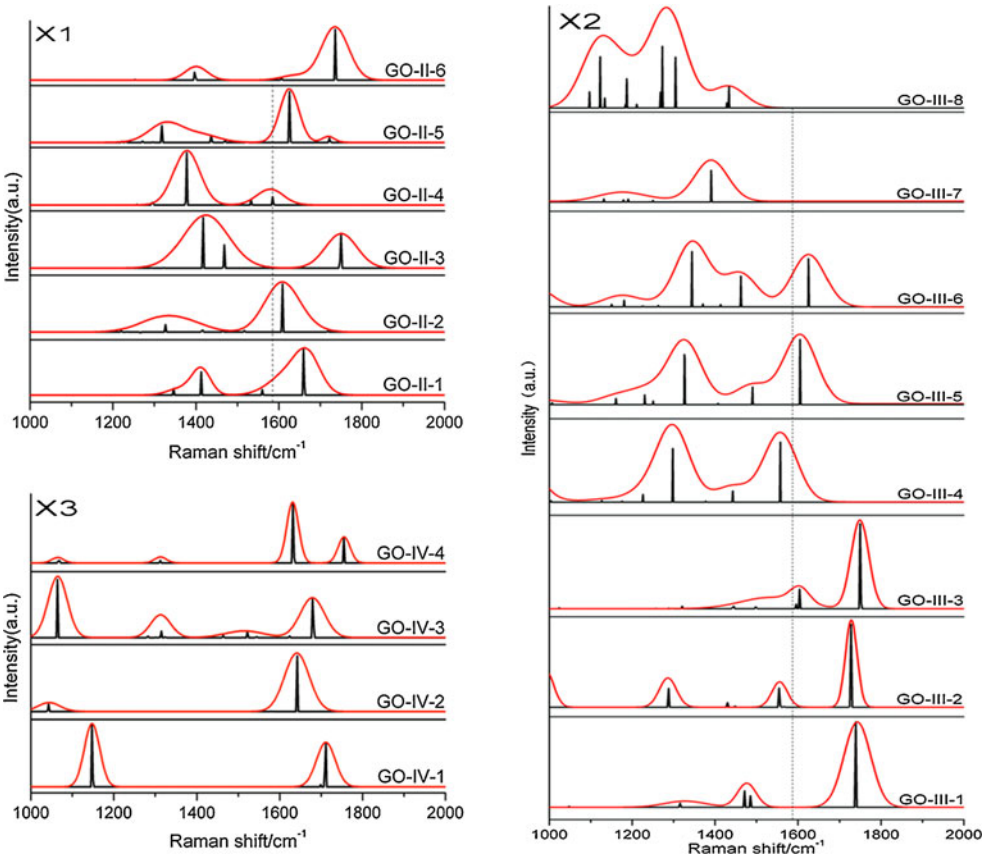

Fig. 4 Raman spectra of different GO models. (X1) Raman spectra of structure with C/O ratio of 4:1. (X2) Raman spectra of structure with C/O ratio of 8:3. (X3) Raman spectra of structure with C/O ratio of 2:1

mode, and the D band is induced by modes split from the A_{1g} mode. For all the above local GO structures, even at the same degree of oxidization, the ID/IG ratio can be considerably different. Among the structures considered (GO-II-4, GO-III-5 and GO-III-6, and GO-IV-2), the GO-II-4 structure has the largest ID/IG ratios of about 4.2, whereas the ID/IG ratios for others are much smaller. It is shown that the ID/IG ratio is a strong function of the local structure. From the Raman spectroscopy view, the GO models with the functional groups arranged close to each other on both sides of graphene surface are more preferable. This is a line with the result of energy analysis, and our studies are consistent with the Bulat's achievement that ortho addition is energetically the most favored [45].

Conclusions

In summary, we have studied the structure and Raman spectra of GO with different arrangements of oxidation functional groups, using DFT method in the local density approximation. We find that the epoxy groups changes the symmetry of the GO, inducing new bands (D bands) in the Raman spectra, which is greatly different from each other. In particular, the symmetry reduction leads to a splitting of the E_{2g} modes of graphene into low symmetry modes which causes the Raman G bands of GO. Therefore, the Raman spectra are related to the oxidation level and the location of the oxidized region. Both structure energy and spectra computations indicate that the oxidation functional groups are energetically favorable to aggregate together and to be close to each other on the opposite side of graphene surface.

Acknowledgments This research used computational resources at the China Academy of Engineering Physics. This work is supported by the National Natural Science Foundation of China (Grant No. 41272051) and the Postgraduate Innovation Fund sponsored by Southwest University of Science and Technology (Grant No.12ycjj22). It is also supported by the Doctoral Fund of Southwest University of Science and Technology (Grant No.11ZX7135).

References

1. Liu F, Ming P, Li J (2007) Phys Rev B 76:064120.1–064120.7
2. Frank IW, Tanenbaum DM, van der Zande AM, McEuen PL (2007) J Vac Sci Tech B 25:2558–2561
3. Novoselov KS, Geim AK, Morozov SV, Jiang D, Zhang Y, Dubonos SV, Grigorieva IV, Firsov AA (2004) Science 306:666–669
4. Nair RR, Blake P, Grigorenko AN, Novoselov KS, Booth TJ, Stauber T, Peres NMR, Geim AK (2008) Science 320:1308–1308
5. Wang F, Zhang YB, Tian CS, Girit C, Zettl A, Crommie M, Shen YR (2008) Science 320:206–209
6. Ghosh S, Calizo I, Teweldebrhan D, Pokatilov EP, Nika DL, Balandin AA, Bao W, Miao F, Lau CN (2008) Appl Phys Lett 92:151911.1–151911.3
7. Balandin AA, Ghosh S, Bao WZ, Calizo I, Teweldebrhan D, Miao F, Lau CN (2008) Nano Lett 8:902–907
8. Geim AK, Novoselov KS (2007) Nat Mat 6:183–191
9. Landau LD (1937) Phys Z Sowjetunion 11:26–35
10. Peierls R (1935) Ann Inst Henri Poincare 5:177–182
11. Lahaye RJWE, Jeong HK, Park CY, Lee YH (2009) Phys Rev B 79:125435.1–125435.8
12. Dinh LD, Gunn K, Kyung JH, Young HL (2010) Phys Chem Chem Phys 12:1595–1599
13. Fuente E, Menéndez JA, Díez MA, Suárez D, Montes-Morán MA (2003) J Phys Chem B 107:6350–6359
14. Kudin KN, Ozbas B, Schniepp HC, Prud'homme RK, Aksay IA, Car R (2008) Nano Lett 8:36–41
15. Li ZY, Zhang WH, Luo Y, Yang JL, Hou JG (2009) J Am Chem Soc 131:6320–6321
16. Pandey D, Reifenberger R, Piner R (2008) Surf Sci 602:1607–1613
17. Li JL, Kudin KN, McAllister MJ, Prud'homme RK, Aksay IA, Car R (2006) Phys Rev Lett 96:176101.1–176101.4
18. Hofmann U, Holst R (1939) Ber Dtsch Chem Ges 72:754–771
19. Buchsteiner A, Lerf A, Pieper J (2006) J Phys Chem B 110:22328–22338
20. Boukhvalov DW, Katsnelson MI (2008) J Am Chem Soc 130:10697–10701
21. Segall MD, Lindan PLD, Probert MJ, Pickard CJ, Hasnip PJ, Clark SJ, Payne MC (2002) J Phys Condens Matter 14:2717–2744
22. Vosko SJ, Wilk L, Nusair M (1980) Can J Phys 58:1200–1211
23. Ceperley DM, Alder BJ (1980) Phys Rev Lett 45:566–569
24. Perdew JP, Zunger A (1981) Phys Rev B 23:5048–5079
25. Ooi N, Rairkar A, Adams JB (2006) Carbon 44:231–242
26. Qin W, Li X, Bian WW, Fan XJ, Qi JY (2010) Biomaterials 31:1007–1016
27. Yan JA, Ruan WY, Chou MY (2008) Phys Rev B 77:125401.1–125401.7
28. Yan JA, Xian L, Chou MY (2009) Phys Rev Lett 103:086802.1–086802.4
29. Xu Z, Xue K (2010) Nanotechnology 21:045704–045707
30. Hernández Rosas JJ, Ramírez Gutiérrez RE, Escobedo-Morales A, Chigo Anota E (2011) J Mol Model 17:1133–1139
31. Hamann DR, Schlüter M, Chiang C (1979) Phys Rev Lett 43:1494–1497
32. Monkhorst HJ, Pack JD (1976) Phys Rev B 13:5188–5192
33. Fischer TH, Almlof J (1992) J Phys Chem 96:9768–9774
34. He H, Klinowski J, Forster M, Lerf A (1998) Chem Phys Lett 287:53–56
35. Lerf A, He H, Forster M, Klinowski J (1998) J Phys Chem B 102:4477–4482
36. Cai W, Piner RD, Stadermann FJ, Park S, Shaibat MA, Ishii Y, Yang D, Velamakanni A, An SJ, Stoller M, An J, Chen D, Ruoff RS (2008) Science 321:1815–1817
37. Yan JA, Chou MY (2010) Phys Rev B 82:125403.1–125403.10
38. Stankovich S, Dikin DA, Piner R, Kohlhaas KM, Kleinhammes A, Jia Y, Wu Y, Nguyen ST, Ruoff RS (2007) Carbon 45:1558–1565
39. Lambert TN, Luhrs CC, Chavez CA, Wakeland S, Brumbach MT, Alam TM (2010) Carbon 48:4081–4089
40. Ferrari AC, Robertson J (2000) Phys Rev B 61:14095–14107
41. Akhavan O (2010) Carbon 48:509–519
42. Zhu Y, Murali S, Cai W, Li X, Suk JW, Potts JR, Ruoff RS (2010) Adv Mater 22:3906–3924
43. Ferrari AC, Meyer JC, Scardaci V, Casiraghi C, Lazzeri M, Mauri F, Piscanec S, Jiang D, Novoselov KS, Roth S, Geim AK (2006) Phys Rev Lett 97:187401.1–187401.4
44. Graf D, Molitor F, Ensslin K, Stampfer C, Jungen A, Hierold C, Wirtz L (2007) Nano Lett 7:238–242
45. Bulat FA, Burgess JS, Matis BR, Baldwin JW, Macaveiu L, Murray JS, Politzer P (2012) J Phys Chem A 116:8644–8652